ATLANTIS PRESS

Advances in Computer Science Research, volume 86

International Symposium on Communication Engineering & Computer Science (CECS 2018)

A 3D CFD Simulation and Analysis of Flow-induced Forces on Quartz Crystal Microbalance Sensor in Solution with Different Temperatures

Huatao Wang[a], Bin Xie[b] and Fenhua Wang[*,c]

School of Automation and Electrical Engineering, University of Science and Technology Beijing, Beijing 100083, China

[a]wanghuataovictor@163.com, [b]15810856129@163.com, [c,*]wangfenhua@ustb.edu.cn

Abstract. Quartz crystal microbalance (QCM) is a very powerful method that can measure a mass variation per unit area by measuring the change in frequency of a quartz crystal sensor. The hybrid temperature effect on a QCM sensor in solution leads to unconvincing detection results. A 3D Computational fluid dynamics (CFD) simulation and analysis was conducted to display the 3D nature of the geometric model of the QCM sensor in NaCl solution with different temperatures. We found the relationships among the resultant forces (Fy), the compensatory frequency calculated by the improved Sauerbrey equation and the temperature of NaCl solution. The results show the hybrid temperature effect has an influence on the flow-induced forces, which cause the vibration frequency drift of QCM sensor. This plays a significant reference role in enhancing the accuracy and stability of the QCM measurements when the QCM sensor used in solution.

Keywords: Computational fluid dynamics, Quartz crystal microbalance, Flow-induced forces.

1. Introduction

Quartz crystal microbalance (QCM) is a very powerful method that can measure a mass variation per unit area by measuring the change in frequency of a quartz crystal sensor. The changes of mass deposited on the crystal surface are directly reflected in changes of sensor frequency[1]. When a QCM sensor contacts liquids, the frequency shift has contributions from both rigid mass accumulation and liquid property changes, e.g. density and viscosity[2]. The density and viscosity of solutions have strong dependence with temperature[3]. Thus, the temperature effect in the QCM measurement cannot be neglected as an important factor. Bechmann R proposed the relationship between frequency change of QCM and temperature, which can be developed in a power series[4]. Gu et al. proposed an empirical equation that can be used to effectively compensate the drift of the QCM sensor in aqueous solution[5]. However, the above conclusions were only from experiment results, which have the nature of subjectivity and unconvincingly. Computational fluid dynamics (CFD) is a branch of fluid mechanics that uses numerical analysis and data structures to solve and analyze problems that involve fluid flows[6]. Athanasia M et al. utilized CFD software to investigate the effect of influent temperature variations in a sedimentation tank for potable water treatment and the results showed that the buoyancy of the tank rises with the increase of temperature[7]. A. I. Mizev et al. investigated the characteristics of the forces on the thermal capillary in silicone oil with different temperatures[8]. D Nezar et al. applied a CFD software to study how the temperature affects the forces on the formation of convective patterns in a horizontal liquid layer[9].

In this paper, a 3D CFD simulation and analysis was conducted to display the 3D nature of the geometric model of the QCM sensor in NaCl solution with different temperatures. The results are presented by means of the static pressure distribution and the resultant forces on the QCM sensor under different temperatures.

2. Assumption Define and Model Geometric

2.1 Assumption Define

This study focused on the influence of hybrid temperature effect to the flow-induced forces on the QCM sensor in solution. In this work, a 8-MHz AT-cut QCM (AC8AP14, JJK Electronic Co., Ltd.,)

coated with gold were used. And its frequency measurement was 7.965283MHz by using a frequency measuring device (EQCM-400C, Shanghai, Instruments, Inc.). Before setting up the model, some assumptions are formulated [10]:

Assumption 1 The QCM sensor's oscillatory vibration motion is neglected; this is justifiable as a first approximation since the vibration amplitude of QCM sensor is relatively small at high frequencies.

Assumption 2 Under the above simplification, the inertia forces inherent in the resonance motion of the QCM sensor were not taken into account.

2.2 Geometric Model

Fig. 1(a) and Fig. 2(a) show the QCM sensor and the electrolytic cell that we used in this work, respectively. The geometric model of the QCM sensor as shown in Fig. 1(b), the geometric parameters are gives as d1 = 14mm and d2 = 8mm, respectively. Fig. 2(b) shows the geometric model of the electrolytic cell, the geometric parameters are gives as h1 = 5mm, h2 = 3mm, h3 = 7mm, h4 = 36mm, h5 = 8mm, d3 = 34mm, d4 = 20mm, d5 = 14mm, d6 = 7mm, and d7 = 2mm.

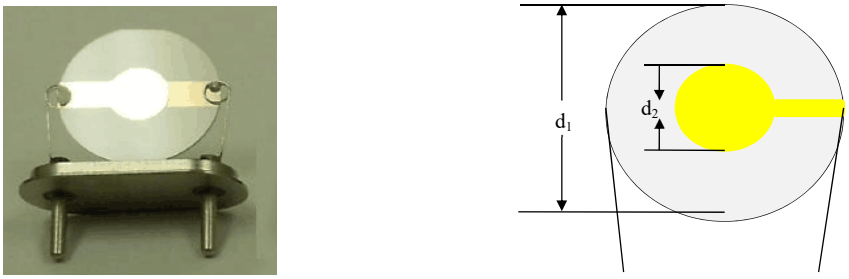

(a) (b)

Fig. 1 (a) Photo of the QCM sensor (b) The geometric model of the QCM sensor

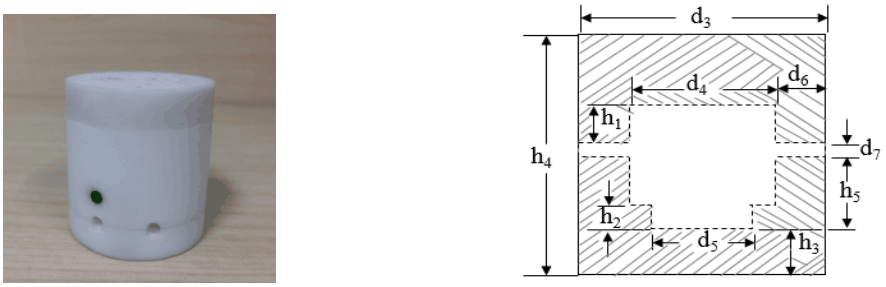

(a) (b)

Fig. 2 (a) Photo of the electrolytic cell (b) The geometric model of the electrolytic cell

3. CFD Modeling

A 3D CFD simulation and analysis in ANSYS Fluent 16.0 (ANSYS, Pittsburgh, PA, USA) software was conducted to display the 3D nature of the geometric model of the QCM sensor in NaCl solution.

3.1 Governing Equations in CFD

The heat conduction differential equation and the governing equations of conservations of mass, momentum, and energy are expressed as follows.

$$\frac{\partial u}{\partial x}+\frac{\partial v}{\partial y}+\frac{\partial w}{\partial z}=0 \tag{1}$$

$$\frac{\partial u}{\partial t}+u\frac{\partial u}{\partial x}+v\frac{\partial u}{\partial y}+w\frac{\partial u}{\partial z}=-\frac{1}{\rho}\frac{\partial p}{\partial x}+\frac{\mu}{\rho}\left(\frac{\partial^2 u}{\partial x^2}+\frac{\partial^2 u}{\partial y^2}+\frac{\partial^2 u}{\partial z^2}\right) \tag{2}$$

$$\frac{\partial v}{\partial t}+u\frac{\partial v}{\partial x}+v\frac{\partial v}{\partial y}+w\frac{\partial v}{\partial z}=-\frac{1}{\rho}\frac{\partial p}{\partial y}+\frac{\mu}{\rho}(\frac{\partial^2 v}{\partial x^2}+\frac{\partial^2 v}{\partial y^2}+\frac{\partial^2 v}{\partial z^2}) \tag{3}$$

$$\frac{\partial w}{\partial t}+u\frac{\partial w}{\partial x}+v\frac{\partial w}{\partial y}+w\frac{\partial w}{\partial z}=-\frac{1}{\rho}\frac{\partial p}{\partial z}+\frac{\mu}{\rho}(\frac{\partial^2 w}{\partial x^2}+\frac{\partial^2 w}{\partial y^2}+\frac{\partial^2 w}{\partial z^2}) \tag{4}$$

$$\frac{\partial(c_pT)}{\partial t}+u\frac{\partial(c_pT)}{\partial x}+v\frac{\partial(c_pT)}{\partial y}+w\frac{\partial(c_pT)}{\partial z}=\frac{\partial}{\partial x}\left(k\frac{\partial T}{x}\right)+\frac{\partial}{\partial y}\left(k\frac{\partial T}{y}\right)+\frac{\partial}{\partial z}\left(k\frac{\partial T}{z}\right) \tag{5}$$

$$\rho c\frac{\partial t}{\partial \tau}=\frac{\partial t}{\partial x}\left(\lambda\frac{\partial t}{\partial x}\right)+\frac{\partial t}{\partial y}\left(\lambda\frac{\partial t}{\partial y}\right)+\frac{\partial t}{\partial z}\left(\lambda\frac{\partial t}{\partial z}\right)+\Phi \tag{6}$$

Nomenclatures in the governing equations are listed in Table 1.

Table 1. Nomenclatures

Nomenclature			
x	x-th component of the coordinate vector, m	t	time, s
y	y-th component of the coordinate vector, m	p	pressure, Pa
z	z-th component of the coordinate vector, m	ρ	density, kg/m2
u	x-th component of the vector, m/s	T	temperature, °C
v	y-th component of the vector, m/s	c	specific heat, J (kg·K)
w	z-th component of the vector, m/s	λ	thermal conductivity
cp	constant pressure specific heat, kJ/(kg·°C)	Φ	the source term
μ	dynamic viscosity, N·s/m2		

3.2 CFD Approach and Mesh Generation

The CFD approach established the geometric model, mesh generation of the geometric model, numerical computing, and post-processing of the computing results. The integrated computer engineering and manufacturing code for computational fluid dynamics (ICEM CFD, ANSYS, Pittsburgh, PA, USA) software was used in the establishment and mesh generation of the geometric model. During the numerical computing, the finite volume method was employed in discretizing the governing equations, and the discretized algebraic equations were solved iteratively by using the unstructured CFD solver, Fluent 16.0. The CFD-post (ANSYS, Pittsburgh, PA, USA) and Tecplot (Tecplot, USA) software were used in the post-processing step.

Fig. 3 shows the mesh of the geometric model in the computational domain generated by ICEM software from a partial-view. The generated mesh had maximum density near QCM sensor, which decreases smoothly towards the wall of the cavity. The computational domain was meshed to a fine structural tetrahedron mesh, which contained 92,727 nodes and 547,916 tetrahedrons. The mesh was chosen for evaluation of flow-induced forces on QCM sensor after performing steady simulation for a grid independence study. All simulation calculations were carried out by using the mesh.

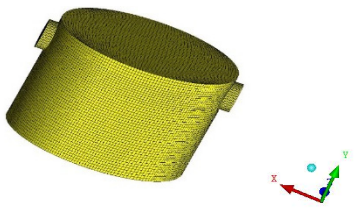

Fig. 3 Schematic of block structured mesh used in this study

3.3 Boundary Conditions

The velocity of the inlet boundary condition was implemented at the inlet of the electrolytic cell and a presumed uniform inlet velocity, 2.1 m/s, corresponding to the real situation at the inlet boundary condition. The type of outlet boundary was set as the pressure-outlet boundary where relative pressure was set to zero in accordance with the real environment. The geometric constraint boundary conditions were set to the walls. The walls and the QCM sensor was maintained at 25℃ (room temperature). Furthermore, the NaCl solution dose not slip onto the walls of the QCM sensor and the walls are impermeable.

3.4 Simulation Strategy

The temperature of the NaCl solution was set to the only independent variable in all simulations. Eight simulations were conducted under eight temperature conditions (see Table 2), respectively. The steady simulation was utilized for studying the grid independence and the unsteady simulation was adopted to model the fluid flow in the electrolytic cell, respectively. The steady state solver was initially run for 1000 iterations with de-creased Under Relaxation Factors (URF) from which residuals start exhibiting periodical oscillations. The steady simulation was then solved by further running the steady solver until the residuals reach to the permissible range. The unsteady simulation was run by cutting over to the second-order implicit unsteady solver with original default URF and constant time step of 0.001 s. The transient runs required 15 iterations per time step to reach the desirable residual value 10-5, and a total number of time steps of 150,000 was used for the full unsteady simulation from 0 s to 10 s.

Table 2. The temperature points of NaCl solution

Temperature/℃							
20	23	25	27	30	33	35	40

4. Results and Discussion

4.1 Static Pressure Distribution

Distribution of static pressure on the QCM sensor surface was studied to analyze the effect of flow-induced forces on the QCM sensor. Fig. 4(a) to (g) show the nephogram of the static pressure values on the QCM sensor surface in the NaCl solution with different temperatures at 4s. Red charts in the figures denote higher static pressure, blue charts represent lower pressure, and gradient colors on behalf of forces between the highest static pressure and the lowest static pressure.

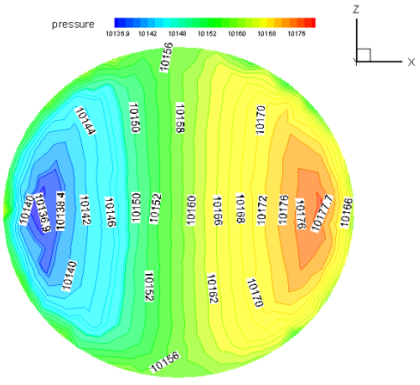

(a)

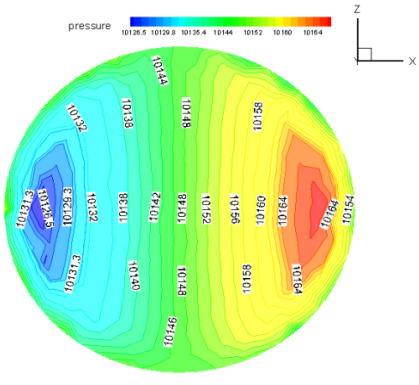

(b)

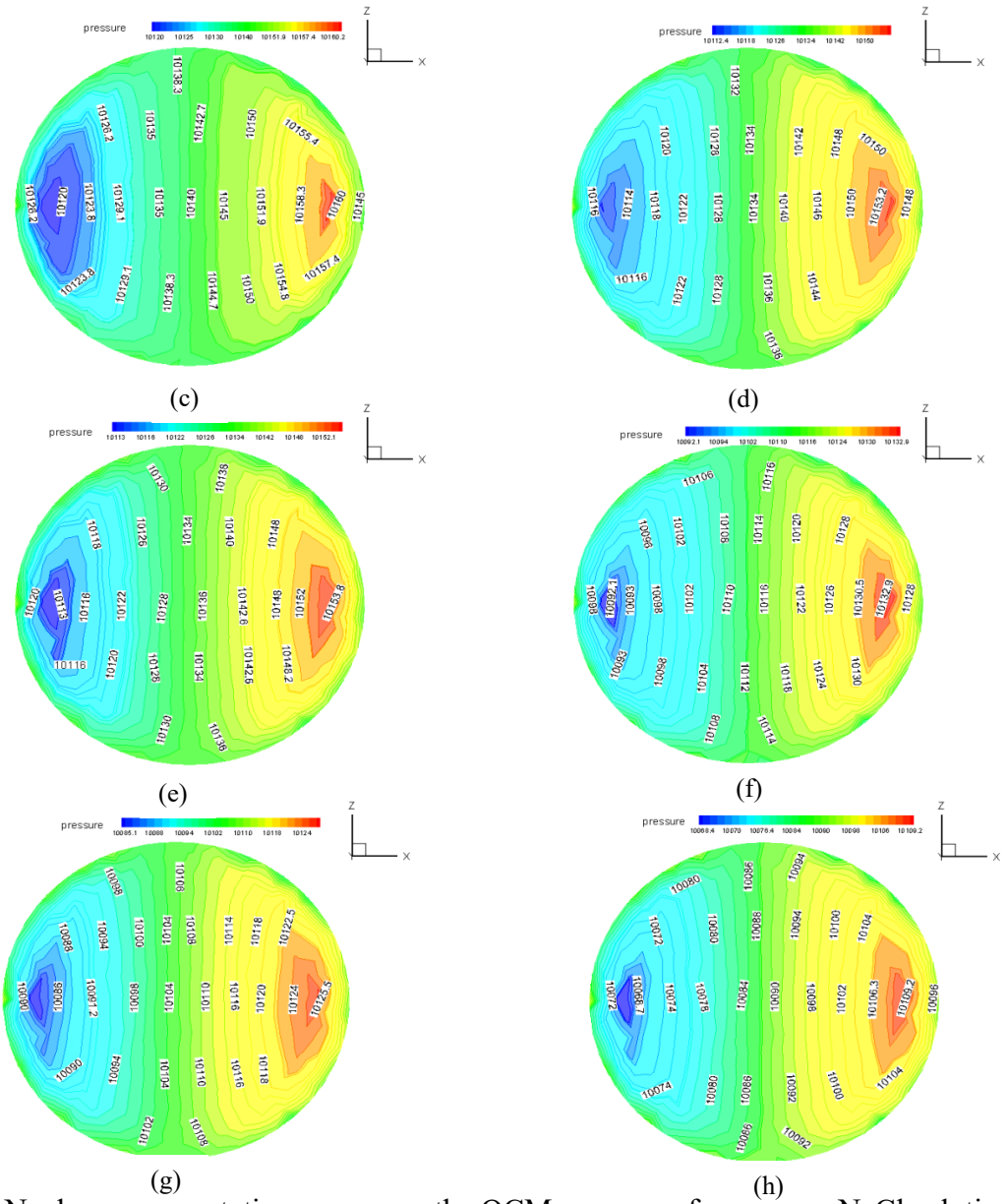

Fig. 4 Nephograms of static pressure on the QCM sensor surfaces in the NaCl solution with different temperatures at 4s: (a) 20°C, (b) 23°C, (c) 25°C, (d) 27°C, (e) 30°C, (f) 33°C, (g) 35°C, and (h) 40°C

Fig. 5 shows the maximum and the minimum static pressures on the QCM sensor surface changed with the temperature of the NaCl solution, respectively.

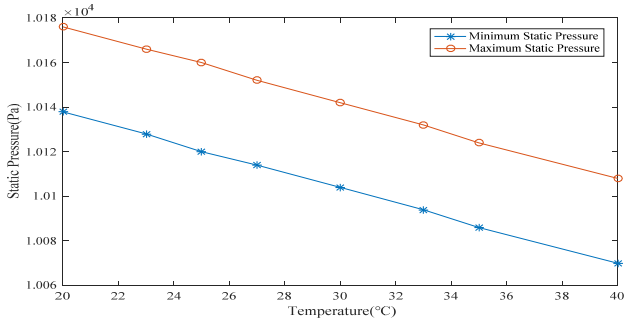

Fig. 5 the maximum and the minimum static pressures on the QCM sensor versus the temperature of the NaCl solution

4.2 Characteristics of Flow-Induced Forces

The unsteady simulation was adopted to model the flow-induced forces in the electrolytic cell. To display the time-varying forces on the QCM sensor, 150,000 resultant force (Fy) values on QCM sensor in the y-direction generalized during the numerical computations from 0s to 10s and the all the values of Fy on the QCM sensor reached a stable value about 2s later.

Fig. 6 shows the Fy on the QCM sensor is decreasing as temperature increases. The Fy have difference among unstable state (1s), critical steady state (2s), stable state (4s), and simulation ending state (10s).

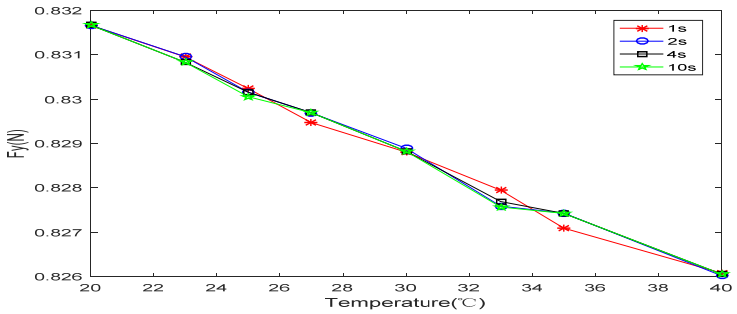

Fig. 6 The Fy versus temperature

Figure. 7 shows the relationships among the Fy, the compensatory frequency (see red line) calculated by the improved Sauerbrey equation and the temperature of NaCl solution[5]. As we can see, when the fluctuations of Fy is stronger, the fluctuations of the resonance frequency values is more obvious. However, when the fluctuations of Fy is not stronger, the fluctuations of the resonance frequency values is affected slightly. This means the hybrid temperature effect has an influence on the Fy, which will cause the vibration frequency drift of QCM sensor.

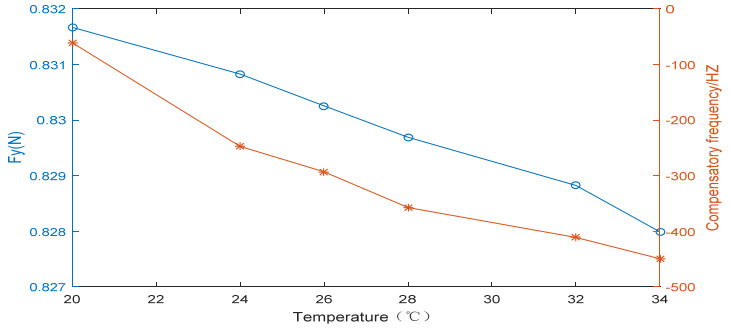

Fig. 7 Blue line chart: The Fy of the QCM sensor, Red line chart: compensatory frequency values of the QCM sensor

5. Summary

In this paper, a 3D CFD simulation using the finite volume method is applied to investigate the flow-induced forces on the QCM sensor in solution with different temperatures. The simulation conclusions demonstrated that both the static pressure and the Fy on the QCM sensor surface were decreased as the temperature of NaCl solution increased. The Fy obtained by the CFD method agree well with the calculation of the improved Sauerbrey equation[5]. Meanwhile, the Fy curve and the compensatory frequency curve variation tendencies were approximate and unanimous. The results show the hybrid temperature effect has an influence on the flow-induced forces, which cause the vibration frequency drift of QCM sensor. Thus, the hybrid temperature effect should be took into account to enhance the accuracy and stability of the QCM measurements when the QCM sensor used in solution.

References

[1]. Ryu D Y, Free M L. The importance of temperature and viscosity effects for surfactant adsorption measurements made using the electrochemical quartz crystal microbalance[J]. Journal of colloid and interface science. Vol. 264 (2003) No. 2, p. 402-406.

[2]. Cao-Paz A M, Marcos-Acevedo J, et al. A multi-point sensor based on optical fiber for the measurement of electrolyte density in lead-acid batteries[J]. Sensors.Vol.2(2010)No. 4, p. 2587-2608.

[3]. Rodríguez H, Brennecke J F. Temperature and composition dependence of the density and viscosity of binary mixtures of water+ ionic liquid[J]. Journal of Chemical & Engineering Data. Vol.51(2006)No. 6, p. 2145-2155.

[4]. Bechmann R. Frequency-temperature-angle characteristics of AT-type resonators made of natural and synthetic quartz[J]. Proceedings of the IRE. Vol.44(1956)No. 11, p. 1600-21607.

[5]. Li Q, Gu Y, Xie B. Hybrid temperature effect on a quartz crystal microbalance resonator in aqueous solutions[J]. Chinese Physics B. Vol.26(2017)No. 6, p. 067704.

[6]. Afzal A, Ansari Z, Faizabadi A R, et al. Parallelization strategies for computational fluid dynamics software: State of the art review[J]. Archives of Computational Methods in Engineering. Vol.24(2017)No. 2,p. 337-363.

[7]. Goula A M, Kostoglou M, Karapantsios T D, et al. The effect of influent temperature variations in a sedimentation tank for potable water treatment—A computational fluid dynamics study[J]. Water research. Vol.42(2008)No. 13, p. 3405-3414.

[8]. Mizev A I, Schwabe D. Convective instabilities in liquid layers with free upper surface under the action of an inclined temperature gradient[J]. Physics of Fluids. Vol.21(2009)No. 11, p. 112102.

[9]. Nezar D, Rahal S. Computational analysis of convective instabilities in a liquid layer subjected to an inclined gradient of temperature[J]. Journal of Applied Mechanics and Technical Physics. Vol.57(2016)No. 3, p. 457-462.

[10]. Gu Y, Wang Y F, Li Q, et al. A 3D CFD simulation and analysis of flow-induced forces on polymer piezoelectric sensors in a Chinese liquors identification e-nose[J]. Sensors. Vol.16(2016)No. 10, p.1738.